Supporting Information for:

Broadband achromatic metasurface-refractive optics

Wei Ting Chen[1], Alexander Y. Zhu[1], Jared Sisler[1,2], Yao-Wei Huang[1,3], Kerolos M. A. Yousef[1,4], Eric Lee[1,2], Cheng-Wei Qiu[3] and Federico Capasso[1,*]

[1]*Harvard John A. Paulson School of Engineering and Applied Sciences, Harvard University, Cambridge, Massachusetts 02138, USA*

[2]*University of Waterloo, Waterloo, ON N2L 3G1, Canada*

[3]*Department of Electrical and Computer Engineering, National University of Singapore, Singapore, 117583, Singapore*

[4]*College of Biotechnology, Misr University for Science and Technology, Giza, Egypt*

*Corresponding author: capasso@seas.harvard.edu

Materials and Methods

Design and simulation. Simulations were performed using 3D finite-difference time-domain method (FDTD solutions from Lumerical Inc.). A large number of elements, each comprising one, two or three nano-fins with different lengths, widths and gaps were simulated under linear *x*-polarized illumination to build up a library. Each element was placed diagonally with respect to the *x*-axis. Periodic and perfectly matched layer boundary conditions were used along the transverse and longitudinal directions, respectively. For each simulation, the y-component of the far-field electric field was recorded as a function of frequency to calculate the phase of each element corresponding to the second term of Eq. 7 in the main text.

To implement the metacorrector, we fit the phase of each element in our library from 460 nm to 700 nm wavelength with a second order polynomial to obtain the group delay and group delay dispersion. Any element that had a R-squared value and polarization conversion efficiency less than 0.98 and 5%, respectively, was dropped. This quadratic fitting with high R-squared values ensures that all selected elements from the library fulfill the desired performance across a wide bandwidth, and that the third order derivatives are zero. Because only the relative phase and dispersion (group delay and group delay dispersion) matter, we applied three different offsets to all elements such that at each spatial coordinate of the metacorrector, the error between the phase/dispersion of a chosen element and the requirements was minimized (obtained by Eq. 3-5 in the main text). The offset values for phase, group delay and group delay dispersion were calculated by a particle swarm algorithm.

Design and simulation of the metacorrector for immersion objective. To design the metacorrector shown in Fig. 5 in the main text we built a simulation model of the objective, including the constituent glass material, thickness and curvature of each individual lens component, using a

commercial software: Zemax OpticsStudio. Due to lack of detailed refractive index information of the immersion oil and the cover glass in the patent (Ref. 45 in the main text), they are assumed to have the same refractive index of 1.52 at λ = 587 nm and Abbe numbers of 41.4 and 58.5, respectively. These numbers were chosen based on Ref. 44 in the main text. We subsequently utilize Zemax to calculate the target frequency-dependent phase profile $\varphi(\mathrm{r},\omega)$ and its group delay, group delay dispersion and the third order dispersion ($\frac{\partial^3\varphi(\mathrm{r},\omega)}{\partial\omega^3}$) accordingly. Finally, we calculate and input the phase profiles at various wavelengths using a Zemax built-in function: "grid phase" to calculate focal length shifts, focal spot profiles and root-mean-square wavefront aberration functions.

Focal spot and imaging measurement. A schematic setup for both measurements is shown in Fig. S4. To characterize the hybrid lens, we use a custom-built microscope consisting of a tunable laser (SuperK and Varia from NKT) and Nikon and Olympus objective lenses (50×, NA = 0.55 and 10×, NA = 0.3). These are paired with their tube lenses (focal length f = 180 and f = 200 mm) and used for point spread function and focal spot measurements, respectively. A pair of crossed linear polarizers was used to reduce background noise in Fig. 3(c), Fig. 3(e), Fig. 4(a) and Fig. 4(b). To measure point spread functions, the 50× objective lens was moved in 5 μm intervals by a motorized stage (Thorlabs, ZST225B), controlled by Labview, to record the intensity distributions along the beam propagation direction on a monochromatic camera (Thorlabs, DCC1545M) for different wavelengths. Subsequently, these images were stacked to obtain Fig. 3(c) and Fig. 3(d).

To compare the focal spot quality for the case with and without the metacorrector, an iris with 1.5 mm diameter which matches the metacorrector diameter was used to reduce the size of the incident beam. The focal spot images in Fig. 3(e) and 3(f) were taken by the 10× objective at

the focal plane of $\lambda = 460$ nm. For imaging measurements, an incoherent light source (Energetiq, EQ-99X LDLS) with various bandpass filters and a condenser was used to illuminate the United States Air Force resolution target. The images in Fig. 4(a) were taken at the focal plane of $\lambda = 458$ nm by a color camera (UI-1540SE, IDS Inc.). The colors of these images were post-processed to match the color of the incident beam. In Fig. 4(b) and 4(c), we show the raw images taken by the color camera. For the case with only the spherical lens (Fig. 4(c)), an iris of 1.5 mm diameter was placed at its back focal plane in order to reduce its aberrated rays to give a fair comparison of chromatic aberration.

Focusing efficiency measurement. In Fig. 3(a), the focusing efficiency as a function of wavelength was measured using a power meter and tunable laser (SuperK and Varia from NKT) with a bandwidth of 10 nm. A pair of crossed linear polarizers was used to remove the background. The power in the focal spot was recorded by the power meter, and normalized to the case without the metacorrector where the polarizers had their axes parallel to each other. The diameter of the incident beam is fixed to 1.5 mm, which is equal to the diameter of the metacorrector.

To measure the focusing efficiency as a function of incident polarizations (Fig. S5), we didn't use any analyzer. Instead, we placed an aperture on the image plane of the custom-built microscope to only allow the center of the focal spot to pass through. The aperture was adjusted to have a diameter equal to the first dark ring of the Airy disk. Subsequently, the power of these focal spots was recorded by a power meter under various incident polarizations and normalized to the power of the focal spot from only the refractive lens. The latter was measured without any aperture to capture all transmitted power.

S1. Focal length shifts of different doublet lenses in the visible region

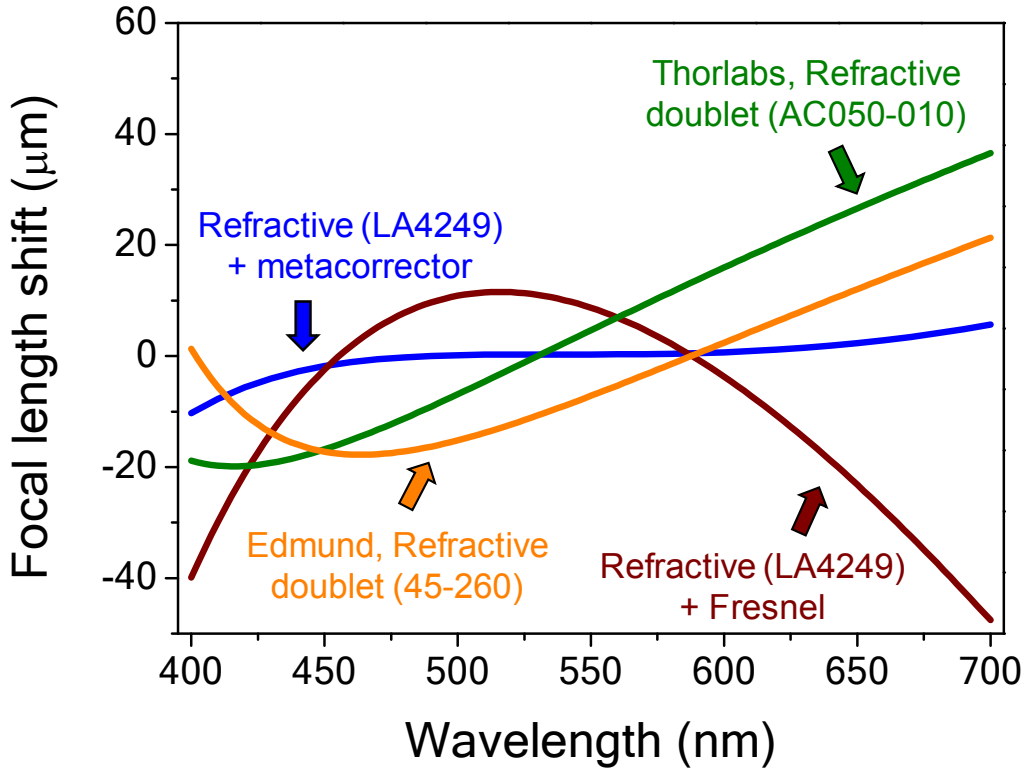

Figure S1: Comparison of chromatic aberration correction using different techniques. The blue curve is the case we showed in Fig. 3(b) in the main text. The brown corresponds to a diffractive Fresnel lens with the same refractive lens. The green and orange curves are refractive doublet lenses designed by Thorlabs and Edmund Inc., respectively. The metacorrector-based doublet has the smallest focal length shift across the visible. To give a fair comparison, all cases have the same entrance pupil diameter of 1.5 mm, NA of 0.075 and focal length of about 10 mm. The model numbers of the refractive lenses are labelled.

S2. Scanning electron microscope images

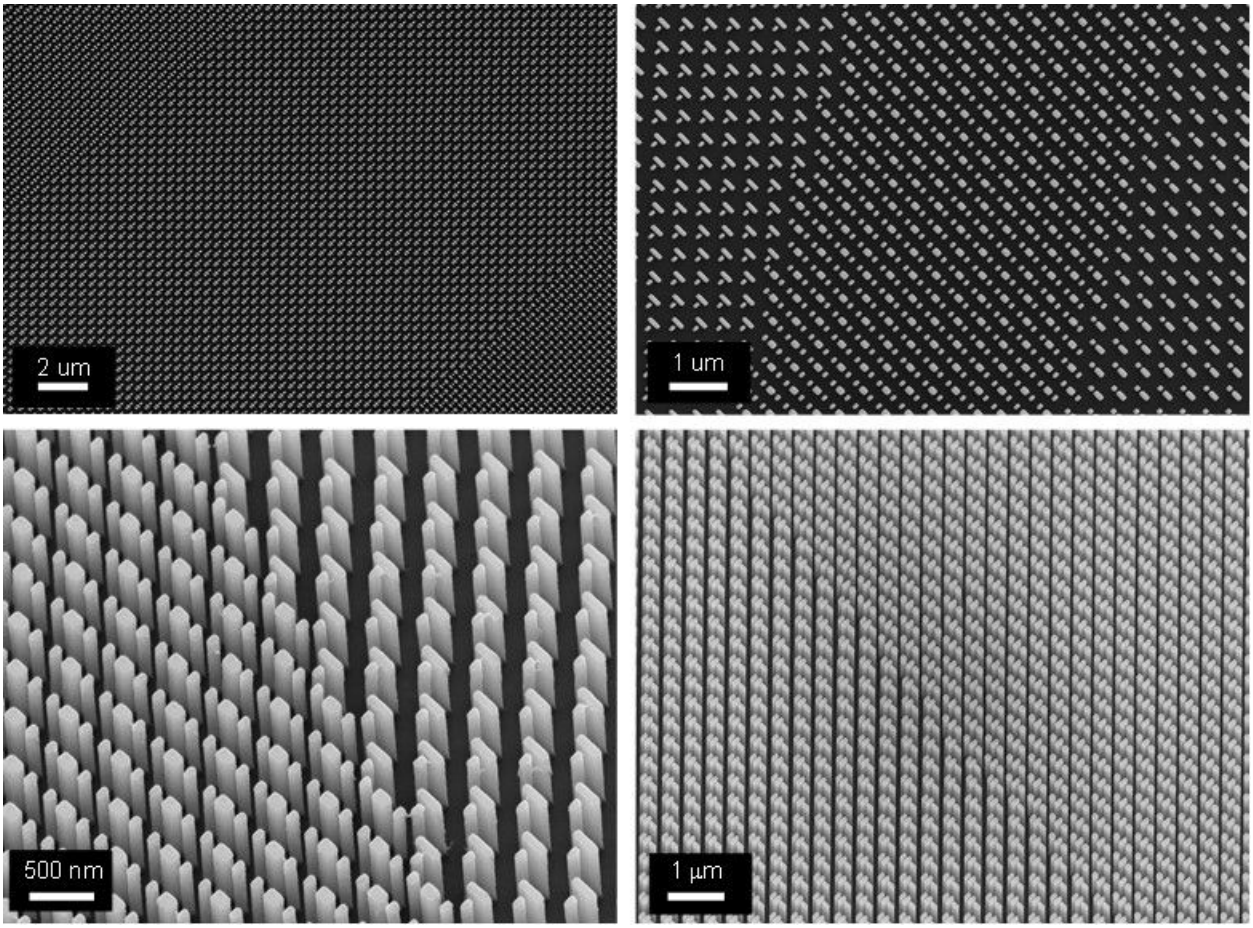

Figure S2: Scanning electron microscope images from different regions of a metacorrector.

S3. Realized phase and dispersion compared to that of required ones

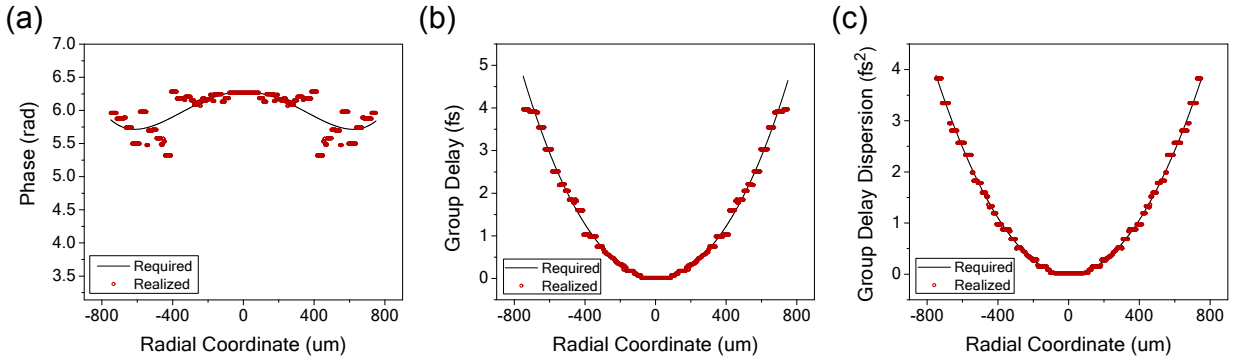

Figure S3: A comparison of phase and dispersion. The red symbols are from different nanostructure elements similar to those shown in the inset of Fig. 1, while the lines are (a) the required phase, (b) group delay and (c) group delay dispersion obtained by Eq. 3 to Eq. 5., respectively. Because the design profiles are radially symmetric, we only show these required values along the horizontal direction across the metacorrector center.

S4. Schematic diagrams of hybrid lens characterization

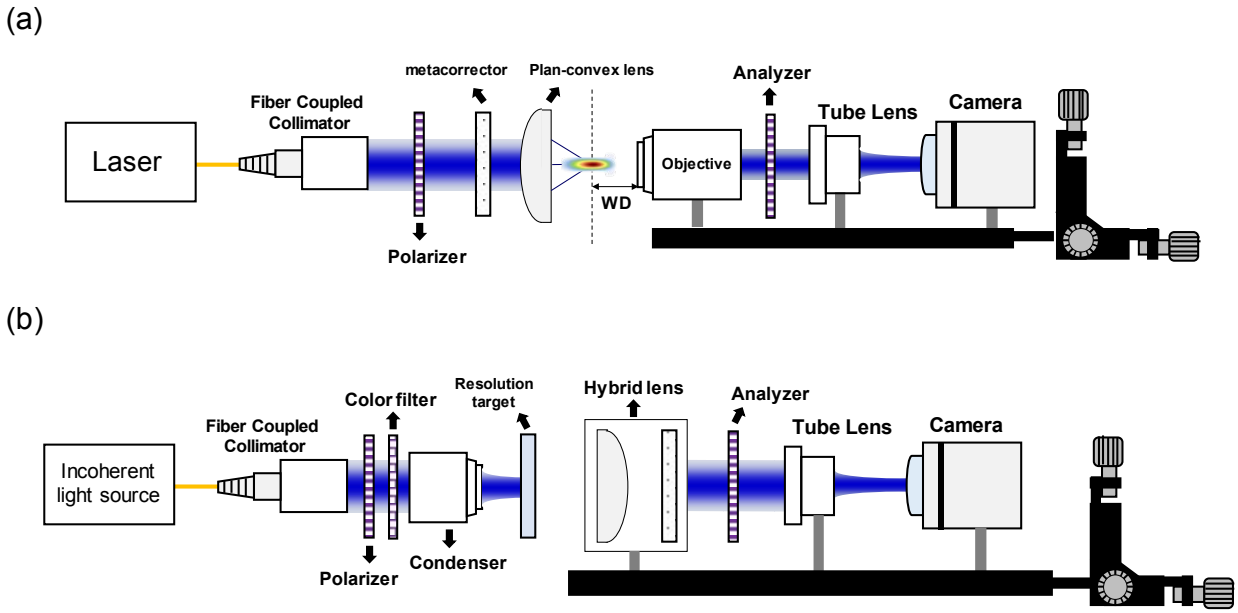

Figure S4: Setups for (a) focal spot and (b) imaging measurements.

S5. Efficiency as a function of polarization

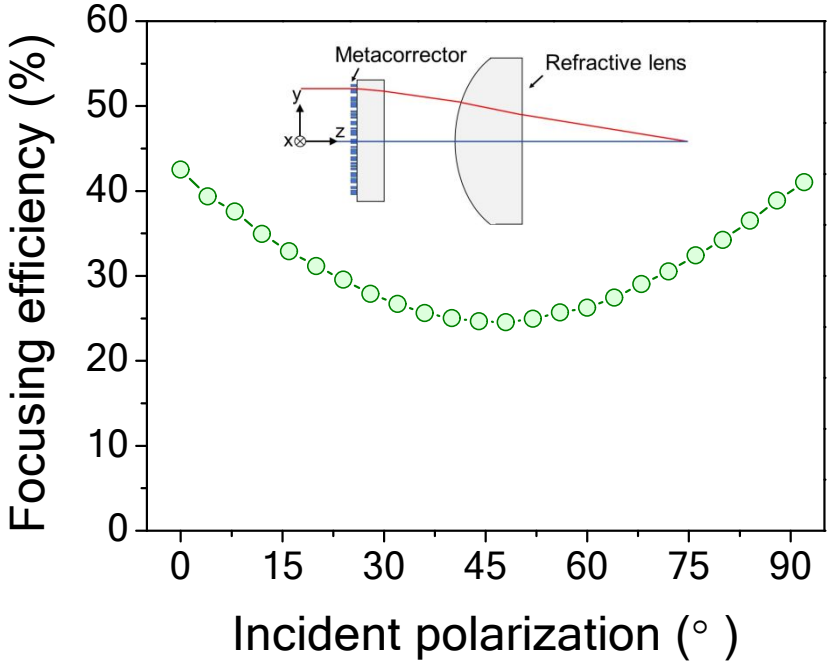

Figure S5: Measured focal spot efficiency of the hybrid lens for different incident linear polarizations at wavelength λ = 500 nm. The focal spot intensity was measured by placing an aperture on the image plane of a microscope to allow only the focal spot to pass through. The aperture size was fixed to be equal to the diameter of the first dark ring of the Airy disk. A power meter was placed behind the aperture to measure focal spot power (normalized to the incident power). The angle of incident linear polarization is defined with respect to *x*-axis (see the inset). The measurement setup is similar to that in Fig. S4(a) without the analyzer and with the camera replaced by the power meter. The efficiency shows a dip at 45º-polarized incidence because of interference. This happens because, at 45º-polarized incidence, the phases of the transmitted light from the first and the second term of Eq. 7 in the main text have the same polarization state. However, this interference effect can be avoided by designing each nanofin element as a miniature half waveplate to minizine the amplitude of the first term.

S6. Comparison of focal spot quality

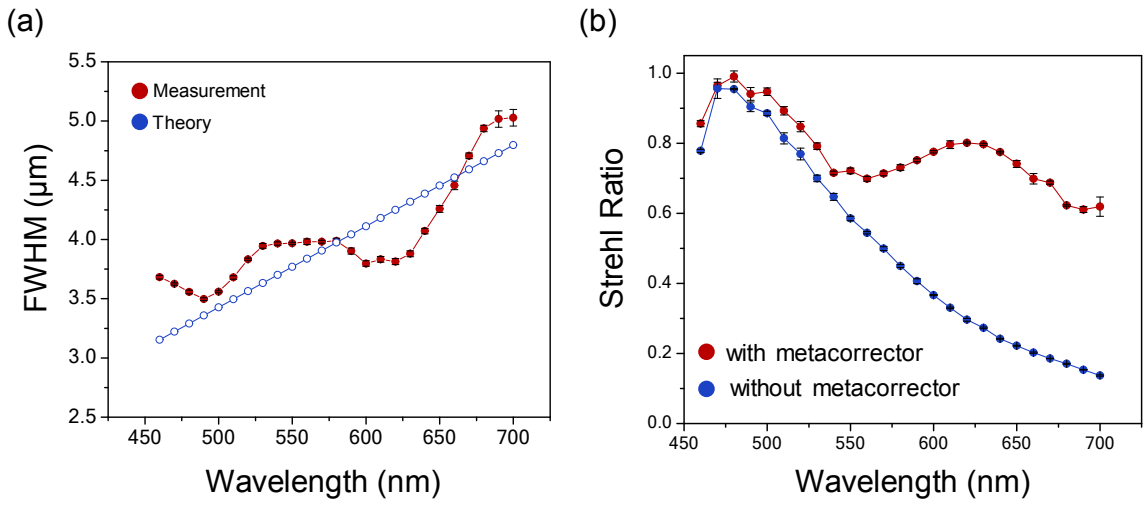

Figure S6: Measured focal spot full-width at half-maximum and Strehl Ratio. (a) Measured and theoretical (diffraction-limited) focal spot full-width at half-maximum (FWHM) values for the hybrid lens. The red and blue circles represent measured and diffraction-limited values respectively. The theoretical diffraction-limited FWHM values were obtained from the formula: $FWHM = 0.514\frac{\lambda}{NA}$. The FWHM calculations used a constant NA = 0.075. The deviation results from the imperfections in realizing phase and dispersion simultaneously. (b) Calculated Strehl ratio values with and without the designed metacorrector. The red and blue circles show the average Strehl ratio with and without the metacorrector, respectively. The error bars span two standard deviations for both plots.

S7. Spectrum of incoherent light source

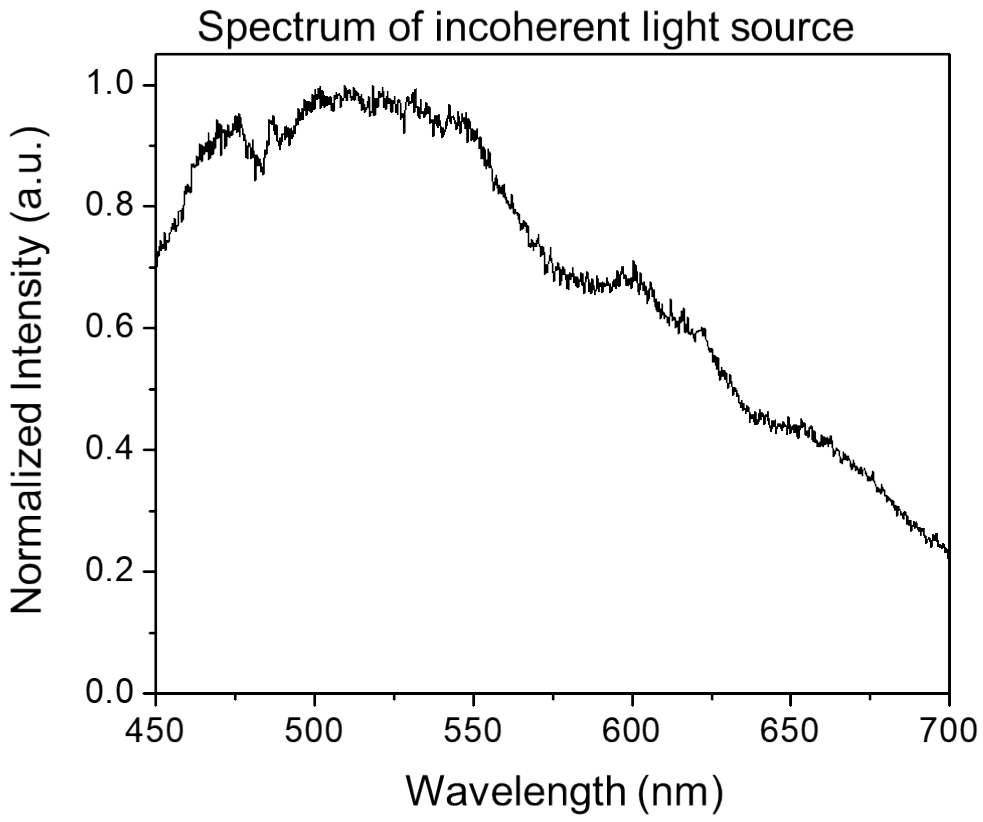

Figure S7: Spectrum of incoherent light source used for imaging in Fig. 4. The spectrum of the light source (EQ-99XFC LDLS, Energetiq) was measured by a spectrometer (USB4000-UV-VIS, Ocean Optics).

S8. Imaging comparison with and without metacorrector

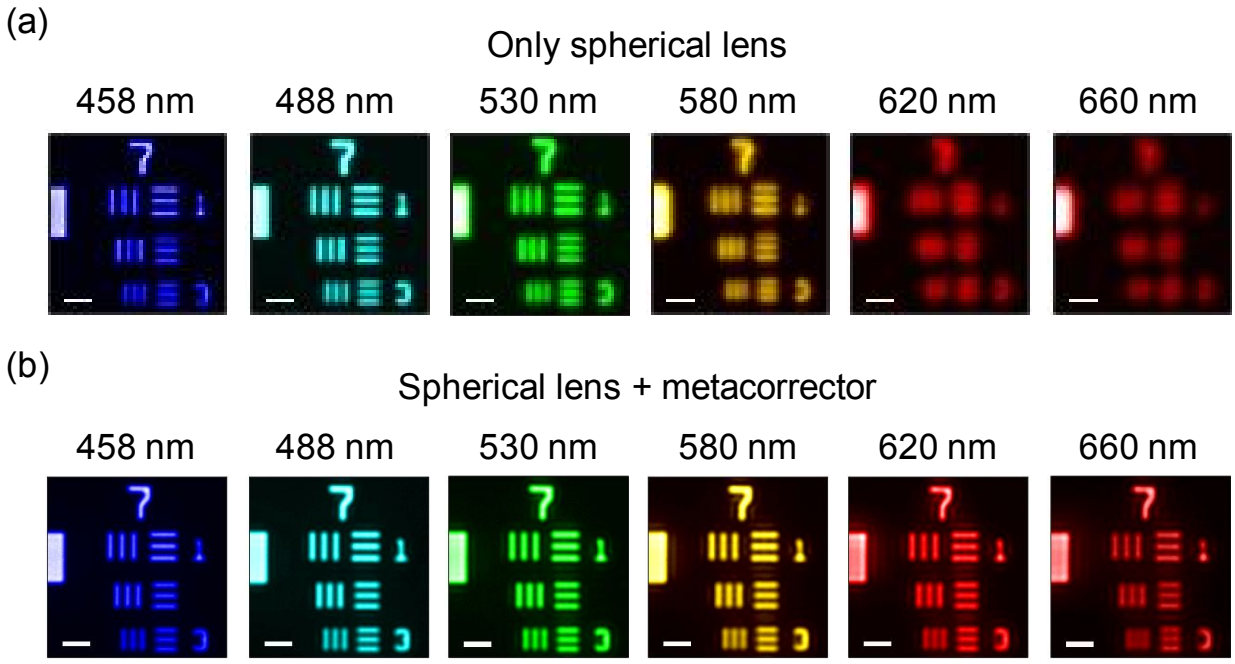

Figure S8: Imaging of the United States Air Force resolution target with and without metacorrector. Images of the United States Air Force resolution target (Thorlabs, R1L1S1N) taken with and without the metacorrector shown in rows (a) and (b), respectively. The camera plane was placed at the focal plane of $\lambda = 458$ nm and kept constant for all other wavelengths. An incoherent light source and various bandpass filters whose center wavelengths are labelled above each image were used to produce the incident light. Without the metacorrector, the images taken by the spherical lens show obvious blurring when the wavelength is larger than 530 nm. Because the spherical lens has a diameter of about 5.5 mm, to give a fair comparison of the chromatic effect, a 1.5 mm dimeter iris (equal in diameter to the metacorrector) was placed at its back focal plane. Scale bars: 15 μm.

S9. Broadband incoherent imaging using the hybrid lens

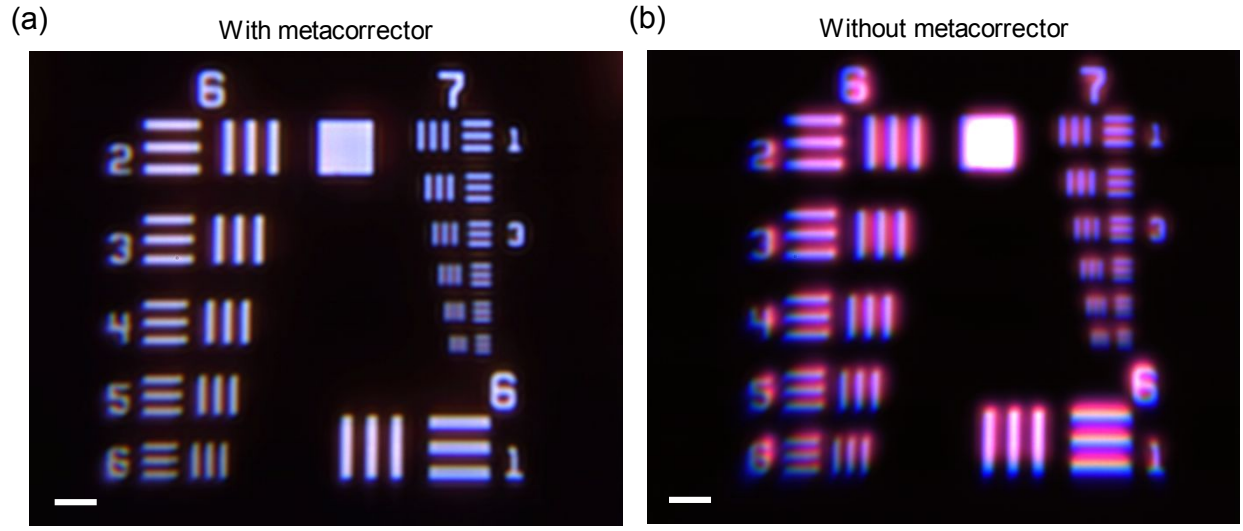

Figure S9: Images of the United States Air Force resolution target under white light illumination. These images were obtained (a) with and (b) without the metacorrector under incoherent light illumination and taken by a color camera. Scale bar: 25 μm. The rainbow tail and blurring are characteristic signs of chromatic aberration of the singlet spherical lens. The rainbow tail of each pattern points along different directions because the center of the lens is located around the first pattern of group 7. This chromatic aberration is well-corrected by the metacorrector. Note that there is still a weak lateral color shift in (a) because of the residual chromatic aberration together with other off-axis aberrations in the hybrid metalens.

S10. Root-mean-square wavefront error for the Zeiss objective with metacorrector

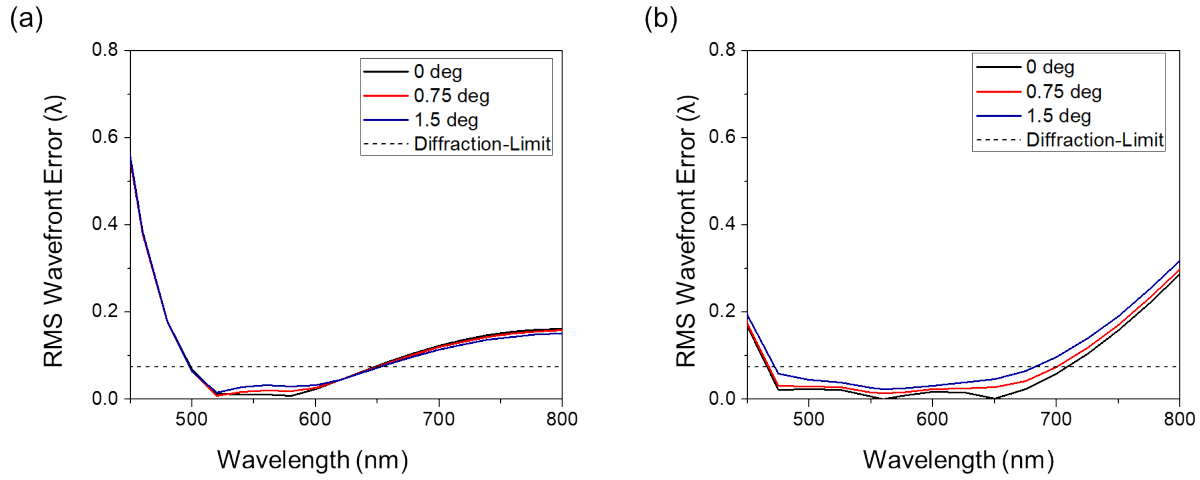

Figure S10: Root-mean-square wavefront aberration function for the objective shown in Fig. 5(a). (a) Root-mean-square (RMS) wave aberration function without the designed metacorrector. (b) RMS wave aberration function with the designed metacorrector. In both plots, different angles of incident light are represented by colored lines and are labelled in the legend. The dotted line in each plot corresponds to an RMS wave aberration function of 0.075 and values below this represent the diffraction-limit. In both (a) and (b), the colors represent the RMS wave aberration functions under different angles of incidence.